Measurement of Muon Antineutrino Quasi-Elastic Scattering on a Hydrocarbon Target at $E_\nu \sim 3.5$ GeV

L. Fields,[1] J. Chvojka,[2] L. Aliaga,[3,4] O. Altinok,[5] A. Bodek,[2] D. Boehnlein,[6] R. Bradford,[2] W.K. Brooks,[7] H. Budd,[2] A. Butkevich,[8] D.A.M. Caicedo,[9] C.M. Castromonte,[9] M.E. Christy,[10] H. da Motta,[9] D.S. Damiani,[3] I. Danko,[11] M. Datta,[10] M. Day,[2] R. DeMaat,[6,*] J. Devan,[3] G.A. Díaz,[4] S.A. Dytman,[11] B. Eberly,[11] D.A. Edmondson,[3] J. Felix,[12] T. Fitzpatrick,[6,*] G.A. Fiorentini,[9] A.M. Gago,[4] H. Gallagher,[5] B. Gobbi,[1,*] R. Gran,[13] D.A. Harris,[6] A. Higuera,[12] I.J. Howley,[3] K. Hurtado,[9,14] M. Jerkins,[15] T. Kafka,[5] M.O. Kanter,[3] C. Keppel,[10] M. Kordosky,[3] A.H. Krajeski,[3] S.A. Kulagin,[8] T. Le,[16] A.G. Leister,[3] G. Maggi,[7,†] E. Maher,[17] S. Manly,[2] W.A. Mann,[5] C.M. Marshall,[2] K.S. McFarland,[2,6] C.L. McGivern,[11] A.M. McGowan,[2] A. Mislivec,[2] J.G. Morfín,[6] J. Mousseau,[18] D. Naples,[11] J.K. Nelson,[3] G. Niculescu,[19] I. Niculescu,[19] N. Ochoa,[4] C.D. O'Connor,[3] J. Osta,[6] J.L. Palomino,[9] V. Paolone,[11] J. Park,[2] C.E. Patrick,[1] G.N. Perdue,[2] C. Peña,[7] L. Rakotondravohitra,[6] R. D. Ransome,[16] H. Ray,[18] L. Ren,[11] P.A. Rodrigues,[2] K.E. Sassin,[3] H. Schellman,[1] D.W. Schmitz,[20,6] R.M. Schneider,[3] E.C. Schulte,[16,‡] P. Sedita,[2] C. Simon,[21] F.D. Snider,[6] M.C. Snyder,[3] J.T. Sobczyk,[22,6] C.J. Solano Salinas,[14] N. Tagg,[23] W. Tan,[10] B.G. Tice,[16] G. Tzanakos,[24,*] J.P. Velásquez,[4] J. Walding,[3,§] T. Walton,[10] J. Wolcott,[2] B.A. Wolthuis,[3] G. Zavala,[12] D. Zhang,[3] and B.P.Ziemer[21]

(The MINERvA Collaboration)

[1] *Northwestern University, Evanston, Illinois 60208*
[2] *University of Rochester, Rochester, New York 14610 USA*
[3] *Department of Physics, College of William & Mary, Williamsburg, Virginia 23187, USA*
[4] *Sección Física, Departamento de Ciencias, Pontificia Universidad Católica del Perú, Apartado 1761, Lima, Perú*
[5] *Physics Department, Tufts University, Medford, Massachusetts 02155, USA*
[6] *Fermi National Accelerator Laboratory, Batavia, Illinois 60510, USA*
[7] *Departamento de Física, Universidad Técnica Federico Santa María, Avda. España 1680 Casilla 110-V, Valparaíso, Chile*
[8] *Institute for Nuclear Research of the Russian Academy of Sciences, 117312 Moscow, Russia*
[9] *Centro Brasileiro de Pesquisas Físicas, Rua Dr. Xavier Sigaud 150, Urca, Rio de Janeiro, RJ, 22290-180, Brazil*
[10] *Hampton University, Dept. of Physics, Hampton, VA 23668, USA*
[11] *Department of Physics and Astronomy, University of Pittsburgh, Pittsburgh, Pennsylvania 15260, USA*
[12] *Campus León y Campus Guanajuato, Universidad de Guanajuato, Lascurain de Retana No. 5, Col. Centro. Guanajuato 36000, Guanajuato México.*
[13] *Department of Physics, University of Minnesota – Duluth, Duluth, Minnesota 55812, USA*
[14] *Universidad Nacional de Ingeniería, Apartado 31139, Lima, Perú*
[15] *Department of Physics, University of Texas, 1 University Station, Austin, Texas 78712, USA*
[16] *Rutgers, The State University of New Jersey, Piscataway, New Jersey 08854, USA*
[17] *Massachusetts College of Liberal Arts, 375 Church Street, North Adams, MA 01247*
[18] *University of Florida, Department of Physics, Gainesville, FL 32611*
[19] *James Madison University, Harrisonburg, Virginia 22807, USA*
[20] *Enrico Fermi Institute, University of Chicago, Chicago, IL 60637 USA*
[21] *Department of Physics and Astronomy, University of California, Irvine, Irvine, California 92697-4575, USA*
[22] *Institute of Theoretical Physics, Wrocław University, Wrocław, Poland*
[23] *Department of Physics, Otterbein University, 1 South Grove Street, Westerville, OH, 43081 USA*
[24] *Department of Physics, University of Athens, GR-15771 Athens, Greece*

(Dated: May 9, 2013)

We have isolated $\bar{\nu}_\mu$ charged-current quasi-elastic interactions occurring in the segmented scintillator tracking region of the MINERvA detector running in the NuMI neutrino beam at Fermilab. We measure the flux-averaged differential cross-section, $d\sigma/dQ^2$, and compare to several theoretical models of quasi-elastic scattering. Good agreement is obtained with a model where the nucleon axial mass, M_A, is set to $0.99\,\mathrm{GeV/c^2}$ but the nucleon vector form factors are modified to account for the observed enhancement, relative to the free nucleon case, of the cross-section for the exchange of transversely polarized photons in electron-nucleus scattering. Our data at higher Q^2 favor this interpretation over an alternative in which the axial mass is increased.

PACS numbers: 13.15.+g,25.30.Pt,21.10.-k

The recent discovery that the neutrino mixing angle $\theta_{13} \approx 9^\circ$ [1–5] makes measuring the hierarchy of neutrino masses and CP violation possible in precision neutrino oscillation experiments. Quasi-elastic interactions,

Operated by Fermi Research Alliance, LLC under Contract No. De-AC02-07CH11359 with the United States Department of Energy.

$\overline{\nu}p \to \ell^+ n$ and $\nu n \to \ell^- p$, have simple kinematics and serve as reference processes in those experiments [1, 6, 7] at GeV energies. These processes are typically modeled as scattering on free nucleons in a relativistic Fermi gas (RFG), with a nucleon axial form factor measured in neutrino-deuterium quasi-elastic scattering [8, 9]. In the RFG model [10] the initial state nucleons are independent in the mean field of the nucleus, and therefore the neutrino energy and momentum transfer Q^2 can be estimated from the polar angle θ_ℓ and momentum p_ℓ of the final state lepton. However, correlations and motion of the initial state nucleons, as well as interactions of the final state particles within the nucleus, significantly modify the Fermi gas picture and affect the neutrino energy reconstruction in oscillation experiments [11–13].

Few measurements of antineutrino quasi-elastic scattering exist [14–16]. The most recent, from the MiniBooNE experiment on a hydrocarbon target at energies near 1 GeV [16], does not agree with expectations based on the RFG model described above. A MiniBooNE analysis of ν_μ quasi-elastic scattering suggests an increased axial form factor at high Q^2 [17]. However, results at higher energy from the NOMAD experiment [18] are consistent with the Fermi gas model and the form factor from deuterium.

In this Letter we report the first study of antineutrino quasi-elastic interactions from the MINERvA experiment, which uses a finely segmented scintillator detector at Fermilab to measure muon antineutrino and neutrino charged current interactions at energies between 1.5 and 10 GeV on nuclear targets. The signal reaction has a μ^+ in the final state along with one or more nucleons (typically with a leading neutron), and no mesons [1]. The μ^+ is identified by a minimum ionizing track that traverses MINERvA [19] and travels downstream to the MINOS magnetized spectrometer [20] where its momentum and charge are measured. The leading neutron, if it interacts, leaves only a fraction of its energy in the detector in the form of scattered low energy protons. To isolate quasi-elastic events from those where mesons are produced, we require the hadronic system recoiling against the muon to have a low energy. That energy is measured in two spatial regions. The *vertex energy* region corresponds to a sphere around the vertex with a radius sufficient to contain a proton (pion) with 120 (65) MeV kinetic energy. This region is sensitive to low energy protons which could arise from correlations among nucleons in the initial state or interactions of the outgoing hadrons inside the target nucleus. We do not use the vertex energy in the event selection. The *recoil energy* region includes energy depositions outside of the vertex region and is sensitive to pions and higher energy nucleons. We use the recoil energy to estimate and remove inelastic backgrounds.

The MINERvA experiment studies neutrinos produced in the NuMI beamline [21] from 120 GeV protons which strike a graphite target. The mesons produced in $p + C$ interactions are focused by two magnetic horns into a 675 m long helium-filled decay pipe. The horns were set to focus negative mesons, resulting in a muon antineutrino enriched beam with a peak energy of 3 GeV. Muons produced in meson decays are absorbed in 240 m of rock downstream of the decay pipe. This analysis uses data taken between November 2010 and February 2011 with 1.014×10^{20} protons on target.

A Geant4-based [22, 23] beamline simulation is used to predict the antineutrino flux. Hadron production in the simulation was tuned to agree with the NA49 measurements of pion production from 158 GeV protons on a thin carbon target [24]. FLUKA is used to translate NA49 measurements to proton energies between 12 and 120 GeV [25, 26]. Interactions not constrained by the NA49 data are predicted using the FTFP hadron shower model [2].

The MINERvA detector consists of a core of scintillator strips surrounded by electromagnetic and hadronic calorimeters on the sides and downstream end of the detector [19][3]. The strips are perpendicular to the z-axis (which is very nearly the beam axis) and are arranged in planes with a 1.7 cm strip-to-strip pitch [4]. Three plane orientations ($0°, \pm 60°$ rotations around the z-axis) enable reconstruction of the neutrino interaction point, the tracks of outgoing charged particles, and calorimetric reconstruction of other particles in the interaction. The 3.0 ns timing resolution is adequate for separating multiple interactions within a single beam spill.

MINERvA is located 2 m upstream of the MINOS near detector, a magnetized iron spectrometer [20]. The MINERvA detector's response is simulated by a tuned Geant4-based [22, 23] program. The energy scale of the detector is set by ensuring that both the photostatistics and the reconstructed energy deposited by momentum-analyzed through-going muons agree in data and simulation. Calorimetric constants used to reconstruct the energy of hadronic showers are determined from the simulation. The uncertainty in the response to single hadrons is constrained by the measurements made with a scaled down version of the MINERvA detector in a low energy hadron test beam [19].

The MINERvA detector records the energy and time

[1] In this analysis quasi-elastic scattering occurs on both free protons and inside carbon nuclei.

[2] FTFP shower model in Geant 4 version 92 patch 03.

[3] The MINERvA scintillator tracking region is 95% CH and 5% other materials by weight.

[4] The y-axis points along the zenith and the beam is directed downward by 58 mrad in the y-z plane.

of energy depositions (hits) in each scintillator strip. Hits are first grouped in time and then clusters of energy are formed by spatially grouping the hits in each scintillator plane. Clusters with energy > 1 MeV are then matched among the three views to create a track. The most upstream cluster on the muon track establishes the event vertex. We identify a μ^+ by matching a track that exits the back of MINERvA with a positively charged track entering the front of MINOS. The per plane track resolution is 2.7 mm and the angular resolution of the muon track is better than 10 mrad [19]. The event vertex is restricted to be within the central 110 planes of the scintillator tracking region and no closer than 22 cm to any edge of the planes. These requirements define a region with a mass of 5.57 metric tons.

The times of the tracked hits are used to determine the interaction time. Other untracked clusters up to 20 ns before and 35 ns after that time are associated with the event. The energy of the recoil system is calculated from all clusters not associated with the muon track or located within the vertex region. Events with two or more spatially contiguous and isolated groups of recoil clusters are rejected as likely being due to inelastic backgrounds.

Event pile-up causes a decrease in the muon track reconstruction efficiency. We studied this in both MINERvA and MINOS by projecting tracks found in one of the detectors to the other and measuring the misreconstruction rate. This resulted in a -7.8% (-4.6%) correction to the simulated efficiency for muons below (above) 3 GeV/c.

Estimation of the initial neutrino energy (E_ν) and four-momentum transfer squared (Q^2) of the interaction assumes an initial state nucleon at rest with a constant binding energy, E_b, which we set to +30 MeV based on electron scattering data [27] and estimates of isospin breaking and Coulomb effects from the semi-empirical mass formula for nuclei [28]. Under this quasi-elastic hypothesis, denoted by QE,

$$E_\nu^{QE} = \frac{m_n^2 - (m_p - E_b)^2 - m_\mu^2 + 2(m_p - E_b)E_\mu}{2(m_p - E_b - E_\mu + p_\mu \cos\theta_\mu)} \quad (1)$$

$$Q^2_{QE} = 2E_\nu^{QE}(E_\mu - p_\mu \cos\theta_\mu) - m_\mu^2, \quad (2)$$

where E_μ and p_μ are the muon energy and momentum, θ_μ is the muon angle with respect to the beam and m_n, m_p and m_μ are the masses of the neutron, proton and muon, respectively.

Figure 1 shows the reconstructed data compared to neutrino interactions simulated using the GENIE 2.6.2 neutrino event generator [29]. For quasi-elastic interactions, the cross-section is given by the Llewellyn Smith formalism [30]. Vector form factors come from fits to electron scattering data [31]; the axial form factor used is a dipole with an axial mass (M_A) of 0.99 GeV/c^2, consistent with deuterium measurements [8, 9]; and subleading form factors are assumed from PCAC or exact

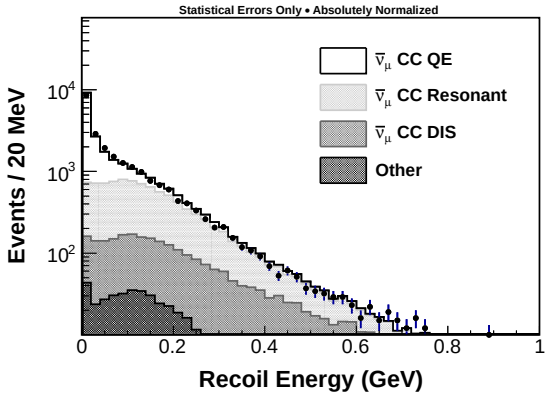

FIG. 1: The measured recoil energy distribution (solid circles) and the predicted composition of signal and background. Backgrounds from baryon resonance production (light grey), continuum/deep-inelastic scattering (dark grey), and other sources (black),such as coherent pion production, are shown.

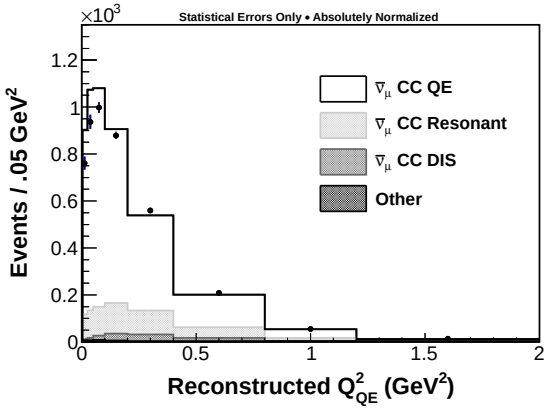

FIG. 2: The measured Q^2_{QE} distribution before background subtraction and corrections for detector resolutions and acceptance.

G-parity symmetry [32]. The nuclear model is the relativistic Fermi gas (RFG) [33] with a Fermi momentum of 221 MeV/c and an extension to higher nucleon momenta to account for short-range correlations [34, 35]. Inelastic reactions with a low invariant mass hadronic final state are based on a tuned model of discrete baryon resonance production [36], and the transition to deep inelastic scattering is simulated using the Bodek-Yang model [37]. Final state interactions, where hadrons interact within the target nucleus, are modeled using the INTRANUKE package [29].

Figure 1 shows evidence of quasi-elastic interactions in the peak of events at low recoil energy. A significant background of inelastic events still exists, primarily from baryon resonance production where the final state pion is not identified. To reduce this background we make

Q^2_{QE} (GeV^2)	I	II	III	IV	V	VI	Total
$0.0 - 0.025$	0.05	0.04	0.00	0.02	0.11	0.02	0.13
$0.025 - 0.05$	0.05	0.04	0.01	0.01	0.11	0.02	0.13
$0.05 - 0.1$	0.05	0.04	0.01	0.01	0.11	0.01	0.13
$0.1 - 0.2$	0.04	0.04	0.01	0.01	0.11	0.01	0.12
$0.2 - 0.4$	0.03	0.06	0.01	0.02	0.11	0.01	0.13
$0.4 - 0.8$	0.05	0.07	0.02	0.03	0.11	0.01	0.15
$0.8 - 1.2$	0.11	0.11	0.02	0.02	0.11	0.02	0.20
$1.2 - 2.0$	0.13	0.15	0.04	0.04	0.12	0.02	0.23

TABLE I: Fractional systematic uncertainties on $d\sigma/dQ^2_{QE}$ associated with muon reconstruction (I), recoil reconstruction (II), neutrino interaction models (III), final state interactions (IV), flux (V) and other sources (VI). The final column shows the total fractional systematic uncertainty due to all sources.

a Q^2_{QE} dependent selection of low recoil-energy events [5]. We also require $E_\nu^{QE} < 10\,\mathrm{GeV}$ to limit uncertainties due to the neutrino flux. Figure 2 shows the Q^2_{QE} distribution of the remaining 16,467 events in the data compared with the simulation.

The background in each Q^2_{QE} bin is estimated from the data by fitting the relative normalizations of signal and background recoil energy distributions whose shapes are taken from the simulation. The fit results in a 10% reduction in the relative background estimate for $Q^2_{QE} > 0.8\,\mathrm{GeV}^2$ and no change to $Q^2_{QE} < 0.8\,\mathrm{GeV}^2$. We then correct for energy resolution using a Bayesian unfolding method [38] with four iterations to produce the event yield as a function of Q^2_{QE}, determined via Eq. 2 with p_μ and θ_μ taken from the GENIE event generator. After unfolding, we use the simulation to correct the yield for efficiency and acceptance, and then divide by the neutrino flux and the number of target nucleons to calculate the bin-averaged cross-section. We estimate the neutrino flux in the range $1.5 \leq E_\nu \leq 10.0\,\mathrm{GeV}$ to be $2.43 \times 10^{-8}\,\mathrm{cm}^{-2}$ per proton on target[6] and there are $1.91 \pm 0.03 \times 10^{30}$ protons in the fiducial volume.

The main sources of systematic uncertainty in the differential cross-section measurement are due to: the reconstruction of the muon; the reconstruction and detector response for hadrons; the neutrino interaction model; final state interactions; and the neutrino flux. These uncertainties are evaluated by repeating the cross-section analysis with systematic shifts applied to the simulation and their effect is shown in Tab. I.

Uncertainties in the muon energy scale have a direct impact on Q^2_{QE} and result in a bin migration of events. The bulk of the uncertainty comes from MINOS, which reconstructs muon energy by range (for stopping tracks) and curvature (exiting). There is a 2.0% uncertainty in the range measurement, due to the material assay and imperfect knowledge of muon energy loss[20]. Using muon tracks which stop in the detector, we compare the momentum measured by range and curvature to establish an additional uncertainty of 0.6% (2.6%) on curvature measurements above (below) 1 GeV/c. We also account for subdominant uncertainties on the energy loss in MINERvA, systematic offsets in the beam angle, mis-modeling of the angular and position resolution, and tracking efficiencies.

The systematic error on the recoil energy measurement is due to the uncertainty in the MINERvA detector energy scale set by muons and differences between the simulated calorimetric response to single hadrons and the response measured by the test beam program. Additional uncertainties are due to differences between the Geant model of neutron interactions and thin target data on neutron scattering in carbon, iron and copper[39–46]. We evaluate further sources of systematic error by loosening analysis cuts on energy near the vertex and on extra isolated energy depositions, repeating the fit to the background and subsequent analysis, and assigning an uncertainty to cover the difference.

Predictions for Q^2_{QE} and recoil energy distributions for neutrino-induced background processes are based upon the GENIE generator. We evaluate the systematic error by varying the underlying model tuning parameters according to their uncertainties [29]. These include parameters governing inelastic interactions of neutrinos with nucleons and those that vary the final state interactions.

The systematic error on the antineutrino flux arises from uncertainties in hadron production in the NuMI target and beamline, and from imperfect modeling of the beamline focusing and geometry [47]. Where hadron production is constrained by NA49 data[24], the NA49 measurement uncertainties dominate. The uncertainty on other interactions is evaluated from the spread between different Geant4 hadron production models [22, 23] The absolute flux uncertainties are large, with a significant E_ν dependence, but mostly cancel in a measurement of the shape of $d\sigma/dQ^2_{QE}$.

The measured differential cross-section $d\sigma/dQ^2_{QE}$ is shown in Fig. 3 and Table II. Averaged over the flux from 1.5 to 10 GeV, we find $\sigma = 0.604 \pm 0.008(\mathrm{stat}) \pm 0.075(\mathrm{syst}) \times 10^{-38}\,\mathrm{cm}^2/\mathrm{proton}$. As noted above, the systematic uncertainties are significantly reduced in the shape of the differential cross-section[7], which is shown in Fig. 4.

[5] The precise selection is $E_{\mathrm{recoil}} < 0.03 + 0.3 \times Q^2_{QE}(\mathrm{GeV}^2/\mathrm{c}^2)$. The Q^2_{QE} dependence improves the signal efficiency for higher Q^2_{QE}.

[6] See Supplemental Material in the Appendix for the flux as a function of energy

[7] See Supplemental Material in Appendix for correlations of the uncertainties among Q^2_{QE} bins for both the cross-section and shape measurement

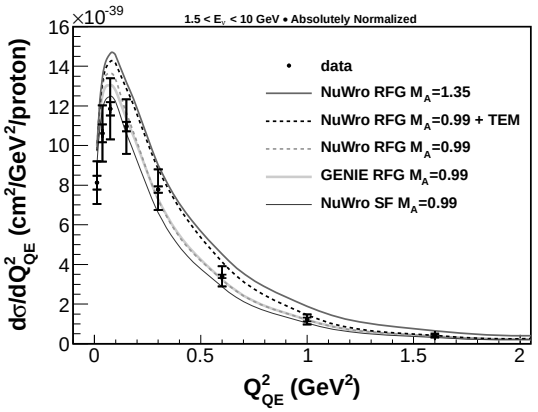

FIG. 3: The anti-neutrino quasi-elastic cross-section as a function of Q^2_{QE} compared with several different models of the interaction described in the text. The inner (outer) error bars correspond to the statistical (total) uncertainties.

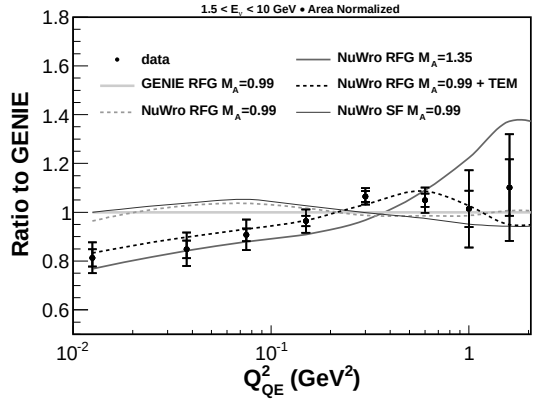

FIG. 4: The data and models of Fig. 3 shown by Q^2_{QE} shape and as a ratio to the reference GENIE prediction.

Table III compares the data to the RFG model in the GENIE event generator and a number of different nuclear models and values of M_A in the NuWro generator [48]. There is little sensitivity to replacement of the Fermi gas with a spectral function (SF) model of the target nucleon energy-momentum relationship [49]. The data disfavor $M_A = 1.35\,\mathrm{GeV}$ as extracted from fits of the MiniBooNE neutrino quasi-elastic data in the RFG model [17]. Our data are consistent with a transverse enhancement model (TEM) which has $M_A = 0.99\,\mathrm{GeV}$ in agreement with deuterium data and includes an enhancement of the magnetic form factors of bound nucleons that has been observed in electron-carbon scattering [50]. The $M_A = 1.35\,\mathrm{GeV}$ and TEM models have a similar Q^2_{QE} dependence at low Q^2_{QE} but are distinguished by the kinematic reach of the data at $Q^2_{QE} > 1\,\mathrm{GeV}^2$.

Transverse enhancement is included as a parametrization affecting the Q^2_{QE} dependence in our analysis but is thought to be due to underlying multinucleon dynamical processes [51–57]. Such processes could have an effect on

Q^2_{QE} (GeV^2)	Cross-section ($10^{-38}\mathrm{cm}^2/\mathrm{GeV}^2/\mathrm{proton}$)	Fraction of Cross-section (%)
$0.0 - 0.025$	$0.813 \pm 0.035 \pm 0.102$	$3.45 \pm 0.15 \pm 0.22$
$0.025 - 0.05$	$1.061 \pm 0.045 \pm 0.134$	$4.50 \pm 0.19 \pm 0.31$
$0.05 - 0.1$	$1.185 \pm 0.033 \pm 0.150$	$10.05 \pm 0.28 \pm 0.63$
$0.1 - 0.2$	$1.096 \pm 0.024 \pm 0.135$	$18.59 \pm 0.41 \pm 0.83$
$0.2 - 0.4$	$0.777 \pm 0.016 \pm 0.101$	$26.38 \pm 0.55 \pm 0.62$
$0.4 - 0.8$	$0.340 \pm 0.009 \pm 0.050$	$23.11 \pm 0.61 \pm 0.98$
$0.8 - 1.2$	$0.123 \pm 0.009 \pm 0.024$	$8.35 \pm 0.61 \pm 1.15$
$1.2 - 2.0$	$0.041 \pm 0.004 \pm 0.010$	$5.57 \pm 0.59 \pm 0.94$

TABLE II: Table of absolute and shape-only cross-section results. In each measurement, the first error is statistical and the second is systematic.

NuWro Model	RFG	RFG +TEM	RFG	SF
M_A (GeV)	0.99	0.99	1.35	0.99
Rate χ^2/d.o.f.	2.64	1.06	2.90	2.14
Shape χ^2/d.o.f.	2.90	0.66	1.73	2.99

TABLE III: Comparisons between the measured $d\sigma/dQ^2_{QE}$ (or its shape in Q^2_{QE}) and different models implemented using the NuWro neutrino event generator, expressed as χ^2 per degree of freedom (d.o.f.) for eight (seven) degrees of freedom. The χ^2 computation in the table accounts for significant correlations between the data points caused by systematic uncertainties.

the vertex and recoil energy distributions that we do not simulate. Motivated by these concerns and by discrepancies observed in our analysis of ν_μ quasi-elastic scattering [58], we have also studied the vertex energy to test the simulation of the number of low energy charged particles emitted in quasi-elastic interactions. Figure 5 shows this energy compared to the simulation. A fit which modifies the distributions to incorporate energy due to additional protons is not able to achieve better agreement. This might be explained if the dominant multibody process is $\bar{\nu}_\mu(np) \to \mu^+ nn$ [59] since MINERvA is not very sensitive to low energy neutrons. We have done a similar analysis on neutrino mode data which indicates additional protons in the final state and is helpful in drawing further conclusions about the effect of the nucleus on quasi-elastic reactions [58].

This work was supported by the Fermi National Accelerator Laboratory under US Department of Energy contract No. DE-AC02-07CH11359 which included the MINERvA construction project. Construction support also was granted by the United States National Science Foundation under Award PHY-0619727 and by the University of Rochester. Support for participating scientists was provided by NSF and DOE (USA) by CAPES and CNPq (Brazil), by CoNaCyT (Mexico), by CONICYT (Chile), by CONCYTEC, DGI-PUCP and IDI/IGI-UNI (Peru), by Latin American Center for Physics (CLAF) and by RAS and the Russian Ministry of Education and Science (Russia). We thank the MINOS Collaboration

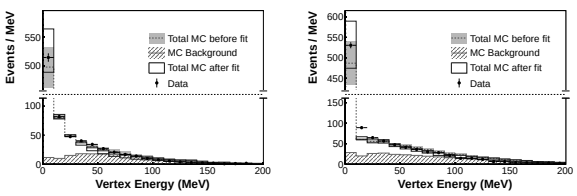

FIG. 5: Reconstructed vertex energy of events passing the selection criteria compared to the GENIE RFG model for $Q^2_{QE} < 0.2$ GeV^2/c^2 (left) and for $Q^2_{QE} > 0.2$ GeV^2/c^2 (right).

for use of its near detector data. Finally, we thank the staff of Fermilab for support of the beamline and the detector.

---

* Deceased
† now at Vrije Universiteit Brussel, Pleinlaan 2, B-1050 Brussels, Belgium
‡ now at Temple University, Philadelphia, Pennsylvania 19122, USA
§ now at Dept. of Physics, Royal Holloway, University of London, UK

[1] K. Abe *et al.* (T2K Collaboration), Phys.Rev.Lett. **107**, 041801 (2011), arXiv:1106.2822 [hep-ex] .
[2] P. Adamson *et al.* (MINOS Collaboration), Phys.Rev.Lett. (2013), arXiv:1301.4581 [hep-ex] .
[3] Y. Abe *et al.* (DOUBLE-CHOOZ Collaboration), Phys.Rev.Lett. **108**, 131801 (2012), arXiv:1112.6353 [hep-ex] .
[4] F. An *et al.* (DAYA-BAY Collaboration), Phys.Rev.Lett. **108**, 171803 (2012), arXiv:1203.1669 [hep-ex] .
[5] J. Ahn *et al.* (RENO Collaboration), Phys.Rev.Lett. **108**, 191802 (2012), arXiv:1204.0626 [hep-ex] .
[6] A. Aguilar-Arevalo *et al.* (MiniBooNE Collaboration), Phys.Rev.Lett. **102**, 101802 (2009), arXiv:0812.2243 [hep-ex] .
[7] D. Ayres *et al.* (NOvA Collaboration), (2004), arXiv:hep-ex/0503053 [hep-ex] .
[8] A. Bodek, S. Avvakumov, R. Bradford, and H. S. Budd, J.Phys.Conf.Ser. **110**, 082004 (2008), arXiv:0709.3538 [hep-ex] .
[9] K. S. Kuzmin, V. V. Lyubushkin, and V. A. Naumov, Eur.Phys.J. **C54**, 517 (2008), arXiv:0712.4384 [hep-ph] .
[10] R. Smith and E. Moniz, Nucl.Phys. **B43**, 605 (1972).
[11] M. Martini, M. Ericson, and G. Chanfray, Phys.Rev. **D87**, 013009 (2013), arXiv:1211.1523 [hep-ph] .
[12] O. Lalakulich and U. Mosel, Phys.Rev. **C86**, 054606 (2012), arXiv:1208.3678 [nucl-th] .
[13] J. Nieves, F. Sanchez, I. Ruiz Simo, and M. Vicente Vacas, Phys.Rev. **D85**, 113008 (2012), arXiv:1204.5404 [hep-ph] .
[14] S. Bonetti, G. Carnesecchi, D. Cavalli, P. Negri, A. Pullia, *et al.*, Nuovo Cim. **A38**, 260 (1977).
[15] L. Ahrens, S. Aronson, B. Gibbard, M. Murtagh, D. White, *et al.*, Phys.Lett. **B202**, 284 (1988).
[16] A. Aguilar-Arevalo *et al.* (MiniBooNE Collaboration), (2013), arXiv:1301.7067 [hep-ex] .
[17] A. Aguilar-Arevalo *et al.* (MiniBooNE Collaboration), Phys.Rev.Lett. **100**, 032301 (2008), arXiv:0706.0926 [hep-ex] .
[18] V. Lyubushkin *et al.* (NOMAD Collaboration), Eur.Phys.J. **C63**, 355 (2009), arXiv:0812.4543 [hep-ex] .
[19] L. Aliaga *et al.* (MINERvA collaboration), FERMILAB-PUB-13-111-E, to be submitted to Nucl. Inst. and Meth .
[20] D. Michael *et al.* (MINOS Collaboration), Nucl.Instrum.Meth. **A596**, 190 (2008), arXiv:0805.3170 [physics.ins-det] .
[21] K. Anderson, B. Bernstein, D. Boehnlein, K. R. Bourkland, S. Childress, *et al.*, *The NuMI Facility Technical Design Report*, FERMILAB-DESIGN-1998-01 (1998).
[22] J. Allison *et al.*, Nuclear Science, IEEE Transactions on **53**, 270 (2006).
[23] S. Agostinelli *et al.*, Nuclear Instruments and Methods in Physics Research Section A: Accelerators, Spectrometers, Detectors and Associated Equipment **506**, 250 (2003).
[24] C. Alt *et al.* (NA49 Collaboration), Eur.Phys.J. **C49**, 897 (2007), arXiv:hep-ex/0606028 [hep-ex] .
[25] A. Ferrari, P. R. Sala, A. Fasso, and J. Ranft, (2005).
[26] G. Battistoni, S. Muraro, P. R. Sala, F. Cerutti, A. Ferrari, *et al.*, AIP Conf.Proc. **896**, 31 (2007).
[27] E. Moniz, I. Sick, R. Whitney, J. Ficenec, R. D. Kephart, *et al.*, Phys.Rev.Lett. **26**, 445 (1971).
[28] T. Katori, *A Measurement of the muon neutrino charged current quasielastic interaction and a test of Lorentz violation with the MiniBooNE experiment*, Ph.D. thesis, Indiana University (2008).
[29] C. Andreopoulos, A. Bell, D. Bhattacharya, F. Cavanna, J. Dobson, S. Dytman, H. Gallagher, P. Guzowski, R. Hatcher, P. Kehayias, A. Meregaglia, D. Naples, G. Pearce, A. Rubbia, M. Whalley, and T. Yang, Nuclear Instruments and Methods in Physics Research Section A: Accelerators, Spectrometers, Detectors and Associated Equipment **614**, 87 (2010).
[30] C. Llewellyn Smith, Phys.Rept. **3**, 261 (1972).
[31] R. Bradford, A. Bodek, H. S. Budd, and J. Arrington, Nucl.Phys.Proc.Suppl. **159**, 127 (2006), arXiv:hep-ex/0602017 [hep-ex] .
[32] M. Day and K. S. McFarland, Phys.Rev. **D86**, 053003 (2012), arXiv:1206.6745 [hep-ph] .
[33] A. Bodek and J. L. Ritchie, Phys. Rev. D **23**, 1070 (1981).
[34] A. Bodek and J. Ritchie, Phys.Rev. **D23**, 1070 (1981).
[35] A. Bodek and J. Ritchie, Phys.Rev. **D24**, 1400 (1981).
[36] D. Rein and L. M. Sehgal, Annals Phys. **133**, 79 (1981).
[37] A. Bodek, I. Park, and U.-k. Yang, Nucl.Phys.Proc.Suppl. **139**, 113 (2005), arXiv:hep-ph/0411202 [hep-ph] .
[38] G. D'Agostini, Nucl.Instrum.Meth. **A362**, 487 (1995).
[39] W. P. Abfalterer, F. B. Bateman, F. S. Dietrich, R. W. Finlay, R. C. Haight, *et al.*, Phys.Rev. **C63**, 044608 (2001).
[40] W. Schimmerling, T. Devlin, W. Johnson, K. Vosburgh, and R. Mischke, Phys.Rev. **C7**, 248 (1973).
[41] R. Voss and R. Wilson, Proc.Roy.Soc. **A236**, 41 (1956).
[42] I. Slypen, V. Corcalciuc, and J. Meulders, Phys.Rev. **C51**, 1303 (1995).
[43] J. Franz, P. Koncz, E. Rossle, C. Sauerwein, H. Schmitt, *et al.*, Nucl.Phys. **A510**, 774 (1990).
[44] U. Tippawan, S. Pomp, J. Blomgren, S. Dangtip, C. Gustavsson, *et al.*, Phys.Rev. **C79**, 064611 (2009), arXiv:0812.0701 [nucl-ex] .

[45] R. Bevilacqua, S. Pomp, M. Hayashi, A. Hjalmarsson, U. Tippawan, *et al.*, (2013), arXiv:1303.4637 [nucl-ex] .
[46] C. Zanelli, P. Urone, J. Romero, F. P. Brady, M. Johnson, *et al.*, Phys.Rev. **C23**, 1015 (1981).
[47] Z. Pavlovic, *Observation of Disappearance of Muon Neutrinos in the NuMI Beam*, Ph.D. thesis, University of Texas (2008).
[48] T. Golan, C. Juszczak, and J. T. Sobczyk, Phys.Rev. **C86**, 015505 (2012), arXiv:1202.4197 [nucl-th] .
[49] O. Benhar, A. Fabrocini, S. Fantoni, and I. Sick, Nucl.Phys. **A579**, 493 (1994).
[50] A. Bodek, H. Budd, and M. Christy, Eur.Phys.J. **C71**, 1726 (2011), arXiv:1106.0340 [hep-ph] .
[51] T. Donnelly and I. Sick, Phys.Rev. **C60**, 065502 (1999), arXiv:nucl-th/9905060 [nucl-th] .
[52] J. Carlson, J. Jourdan, R. Schiavilla, and I. Sick, Phys.Rev. **C65**, 024002 (2002), arXiv:nucl-th/0106047 [nucl-th] .
[53] C. Maieron, J. Amaro, M. Barbaro, J. Caballero, T. Donnelly, *et al.*, Phys.Rev. **C80**, 035504 (2009), arXiv:0907.1841 [nucl-th] .
[54] M. Martini, M. Ericson, G. Chanfray, and J. Marteau, Phys.Rev. **C80**, 065501 (2009), arXiv:0910.2622 [nucl-th] .
[55] J. Amaro, M. Barbaro, J. Caballero, T. Donnelly, and C. Williamson, Phys.Lett. **B696**, 151 (2011), arXiv:1010.1708 [nucl-th] .
[56] M. Martini, M. Ericson, G. Chanfray, and J. Marteau, Phys.Rev. **C81**, 045502 (2010), arXiv:1002.4538 [hep-ph] .
[57] J. Nieves, I. R. Simo, and M. Vicente Vacas, Phys.Lett. **B721**, 90 (2013), arXiv:1302.0703 [hep-ph] .
[58] G. A. Fiorentini, D. W. Schmitz, P. A. Rodrigues, *et al.* (MINERvA collaboration), FERMILAB-PUB-13-146-E, submitted to Phys. Rev. Lett .
[59] R. Subedi, R. Shneor, P. Monaghan, B. Anderson, K. Aniol, *et al.*, Science **320**, 1476 (2008), arXiv:0908.1514 [nucl-ex] .

Appendix: Supplementary Material

Q^2_{QE} (GeV^2) Bins	$0.0-0.025$	$0.025-0.05$	$0.05-0.1$	$0.1-0.2$	$0.2-0.4$	$0.4-0.8$	$0.8-1.2$	$1.2-2.0$
Cross-section in bin	0.813	1.061	1.185	1.096	0.777	0.340	0.123	0.041
(10^{-38}cm^2/GeV^2/proton)	± 0.108	± 0.142	± 0.154	± 0.137	± 0.103	± 0.051	± 0.026	± 0.011
$0.0-0.025$	1.000	0.884	0.911	0.901	0.828	0.700	0.362	0.297
$0.025-0.05$		1.000	0.913	0.904	0.820	0.675	0.343	0.278
$0.05-0.1$			1.000	0.942	0.875	0.726	0.353	0.319
$0.1-0.2$				1.000	0.933	0.825	0.431	0.413
$0.2-0.4$					1.000	0.916	0.541	0.566
$0.4-0.8$						1.000	0.643	0.653
$0.8-1.2$							1.000	0.752
$1.2-2.0$								1.000

TABLE IV: The measurement of the differential cross-sections in Q^2_{QE}, their total (statistical and systematic) uncertainties, and the correlation matrix for these uncertainties

Q^2_{QE} (GeV^2) Bins	$0.0-0.025$	$0.025-0.05$	$0.05-0.1$	$0.1-0.2$	$0.2-0.4$	$0.4-0.8$	$0.8-1.2$	$1.2-2.0$
% of cross-section	3.45	4.50	10.05	18.59	26.38	23.11	8.35	5.57
in bin	±0.27	±0.36	±0.69	±0.93	±0.83	±1.15	±1.30	±1.11
$0.0-0.025$	1.000	0.675	0.722	0.672	0.221	-0.464	-0.440	-0.577
$0.025-0.05$		1.000	0.742	0.716	0.241	-0.517	-0.450	-0.585
$0.05-0.1$			1.000	0.779	0.347	-0.543	-0.562	-0.635
$0.1-0.2$				1.000	0.386	-0.434	-0.627	-0.671
$0.2-0.4$					1.000	-0.051	-0.571	-0.375
$0.4-0.8$						1.000	0.080	0.186
$0.8-1.2$							1.000	0.568
$1.2-2.0$								1.000

TABLE V: The measurement of the *shape* of the differential cross-sections for $Q^2_{QE} < 2.0$ GeV^2, their total (statistical and systematic) uncertainties, and the correlation matrix for these uncertainties

E_ν in Bin	$1.5-2$	$2-2.5$	$2.5-3$	$3-3.5$	$3.5-4$	$4-4.5$	$4.5-5$	$5-5.5$	
$\bar{\nu}_\mu$ Flux (neutrinos/cm^2/POT ($\times 10^{-8}$)	0.281	0.368	0.444	0.448	0.349	0.205	0.106	0.061	
E_ν in Bin	$5.5-6$	$6-6.5$	$6.5-7$	$7-7.5$	$7.5-8$	$8-8.5$	$8.5-9$	$9-9.5$	$9.5-10$
$\bar{\nu}_\mu$ Flux (neutrinos/cm^2/POT ($\times 10^{-8}$)	0.038	0.029	0.022	0.018	0.016	0.013	0.012	0.010	0.009

TABLE VI: The calculated muon antineutrino flux per proton on target (POT) for the data included in this analysis